Journal of Membrane Science 556 (2018) 34–41

Contents lists available at ScienceDirect

Journal of Membrane Science

journal homepage: www.elsevier.com/locate/memsci

Direct numerical simulation of continuous lithium extraction from high Mg^{2+}/Li^{+} ratio brines using microfluidic channels with ion concentration polarization

Lingyan Gong[a], Wei Ouyang[b], Zirui Li[a,*], Jongyoon Han[a,b,c,*]

[a] Institute of Laser and Optoelectronic Intelligent Manufacturing, College of Mechanical and Electrical Engineering, Wenzhou University, Wenzhou 325035, PR China
[b] Department of Electrical Engineering and Computer Science, Massachusetts Institute of Technology, Cambridge, Massachusetts 02139, USA
[c] Department of Biological Engineering, Massachusetts Institute of Technology, Cambridge, Massachusetts 02139, USA

ARTICLE INFO

Keywords:
Ion concentration polarization
Lithium extraction
Electrokinetic trapping
Electroosmotic flow

ABSTRACT

A novel ion concentration polarization-based microfluidic device is proposed for continuous extraction of Li^{+} from high Mg^{2+}/Li^{+} ratio brines. With simultaneous application of the cross-channel voltage that drives electroosmotic flow and the cross-membrane voltage that induces ion depletion, Li^{+} is concentrated much more significantly than other cations in front of the membrane in the microchannel. The application of external pressure produces a fluid flow that drags a portion of Li^{+} (and Na^{+}) to flow through the microchannel, while keeping most of Mg^{2+} (and K^{+}) blocked, thus implementing continuous Li^{+} extraction. Two-dimensional numerical simulation using a microchannel of 120 μm length and 4 μm height and a model, highly concentrated brine, shows that the system may produce a continuous flow rate of 1.72 mm/s, extracting 25.6% of Li^{+}, with a Li^{+}/Mg^{2+} flux ratio of 2.81×10^{3}, at an external pressure of 100 Pa and cross-membrane voltage of 100 times of thermal voltages (25.8 mV). Fundamental mechanisms of the system are elaborated and effects of the cross-membrane voltage and the external pressure are analyzed. These results and findings provide clear guidance for the understanding and designing of microfluidic devices not only for Li^{+} extraction, but also for other ionic or molecular separations.

1. Introduction

Lithium-ion batteries have been widely used in electronics and many other fields since their invention in the last century, due to their high open-circuit voltages, high energy densities, wide operating temperature ranges, etc. [1]. Because of their environmental friendliness, they are substituting the traditional pollution-prone gasoline in the automobile industry. Natural resources of lithium are mainly mineral rocks and lake brines. It has been estimated that about two-thirds of the lithium resources exist in brine of lakes, located in the central Andes and China [2]. Currently, the cost of extracting Li^{+} from brine is lower than that from mineral [3], making extraction of lithium from brines indispensable. One challenge of Li^{+} extraction from brines is the low concentrations of Li^{+}, which is generally less than 100 mM [4]. Another challenge comes from the high Mg^{2+}/Li^{+} ratio, which is generally greater than 40 in the salt lakes of China. Because Mg^{2+} and Li^{+} have similar chemical properties, extraction of lithium while simultaneously removing the more abundant magnesium remains technically difficult.

Currently, there are mainly two classes of lithium extraction technologies: chemical methods [5] and electro-dialysis [6]. Chemical methods extract Li^{+} from brines by precipitation [7,8], solvent extraction [9,10], adsorption [11–13], etc. Although these methods are playing dominant roles in the current Li^{+} extraction industry, they usually suffer from problems of long processing time, large consumption of chemical reagents, membrane fouling, and equipment erosion, etc. [14–17]. Electro-dialysis systems utilize nanofiltration membranes together with ion selective membranes to separate monovalent Li^{+} and Na^{+} from Mg^{2+} [18,19]. Despite the relatively low energy consumption [20] and the environment-friendliness [4], these systems generally suffer from membrane clogging and high cost. In addition, durability of the membranes needs to be enhanced before commercial applications [5]. Overall, the existing extraction techniques are inadequate for most lithium resources [21], and methods based on new mechanisms are of huge demand.

The main interest herein is to develop a novel method to extract lithium from brines of high Mg^{2+}/Li^{+} ratios, based on the ion

* Corresponding author at: Institute of Laser and Optoelectronic Intelligent Manufacturing, College of Mechanical and Electrical Engineering, Wenzhou University, Wenzhou, 32 5035, PR China.
E-mail addresses: lizirui@wzu.edu.cn (Z. Li), jyhan@mit.edu (J. Han).

https://doi.org/10.1016/j.memsci.2018.03.078
Received 25 January 2018; Received in revised form 11 March 2018; Accepted 29 March 2018
Available online 30 March 2018

concentration polarization (ICP) phenomenon using microfluidic channels. Fundamentally, ICP is induced by selective ion transport across nanochannels or ion-exchange membranes [22], or reactions at the electrode surfaces [23]. Accompanying the selective ion transfer, an ion depletion zone with extremely low ion concentrations and amplified electric fields is formed. Combination of ICP and fluid flow facilitates a series of novel applications, such as desalination [24–26], mixing [27,28], biomolecular preconcentration [29–32], and simultaneous separation [33–36]. Here, we use the ICP-induced electric field and the pressure-driven flow to realize flows of Li^+ and Na^+ through the microchannel, while keeping Mg^{2+} and K^+ blocked, thereby realizing continuous-flow extraction of Li^+ from the brine. As the typical three-dimensional (3D) channel size is in the order of tens of micrometers, and ion-exchange membranes in this new device is not responsible for the transport the fluid or Li^+, the system is free from the nanofilter's clogging and low permeability problems. The aim of this paper is to elaborate the fundamental mechanism of the proposed Li^+ extraction device by numerical simulation. Effects of key control parameters, more specifically the cross-membrane voltage and pressure, are clarified.

2. Methods

2.1. System setup

Fig. 1(a) shows the diagram of a two-dimensional (2D) dual-channel ICP-based device for Li^+ extraction. Two horizontal microchannels with positively charged walls are bridged by an anion-exchange membrane (AEM). A cross-membrane upward electric field $\mathbf{E_2}$ is applied to produce the selective transport of anions through the AEM, and generate an ion depletion zone near the AEM in the upper microchannel. The leftward electric field $\mathbf{E_1}$ (facilitating the electroosmotic flow, EOF) and the external pressure P_0 (producing the pressure-driven flow) act together to drive the rightward fluid flow that drags all the charged species into the microchannel. The amplified electric field at the front of the ion depletion zone exerts strong electrophoretic forces on cations and hinders their migrations. For different cation species, balances between the leftward electrophoretic force (proportional to the valence), and the rightward fluid drag force (inverse proportional to the diffusion coefficient) are different, thus their chances of passing through the electric field barrier are different. By calculating the fluxes of different cations under varied electric fields and external pressure, we will demonstrate that Li^+/Mg^{2+} separation may be achieved by permitting only a portion of Li^+ and Na^+ to pass through the microchannel while keeping most Mg^{2+} and K^+ blocked.

Fig. 1(b) shows the schematic computational model for the above system. The key component is a microchannel of length L and height H, with AEM of length L_m embedded in the middle of both the upper and lower walls. The walls of the microchannel are positively charged with a surface charge density σ_+, and AEMs are assumed to permit the passage of anions only. Two wider compartments with length L_1 and height H_1 are connected to left and right ends of the microchannel, representing part of the reservoirs. The channel is filled with the mixed solution of Li^+, Na^+, K^+, Mg^{2+} and Cl^-, simulating the brine. The concentration of Cl^- in the membrane is C_m, which is determined by the requirement to balance the fixed charge density in AEM. Voltages V_L and V_R ($V_L < V_R$) are applied to generate a leftward electric field ($\mathbf{E_1}$ in Fig. 1(a)), which induces an rightward EOF (of the first kind, EOF1). In this sense, the left reservoir is referred to as the inlet reservoir, and the right one as the outlet reservoir. A voltage V_m is applied on the membranes to generate a cross-membrane voltage $V_{cm}=V_m-(V_L+V_R)/2$ ($V_{cm} > 0$, simulating $\mathbf{E_2}$ in Fig. 1(a)). Larger V_{cm} drives more anions out of the microchannel in unit time and induces stronger ion depletion inside it. Pressures at the left boundary and the right boundary are set to P_0 and 0, respectively.

2.2. Governing equations

The governing equations for incompressible fluid flow, transport of ions, and electric potential are the Navier-Stokes, Nernst-Plank, and Poisson equations [37,38], respectively,

$$\rho(\partial\mathbf{U}/\partial t + (\mathbf{U}\cdot\nabla)\mathbf{U}) = -\nabla P + \eta\nabla\cdot\nabla\mathbf{U} - \rho_e\nabla\Phi, \quad (1)$$

$$\nabla\cdot\mathbf{U} = 0, \quad (2)$$

$$\frac{\partial C_i}{\partial t} = -\nabla\cdot\ \mathbf{J}_i, \quad (3)$$

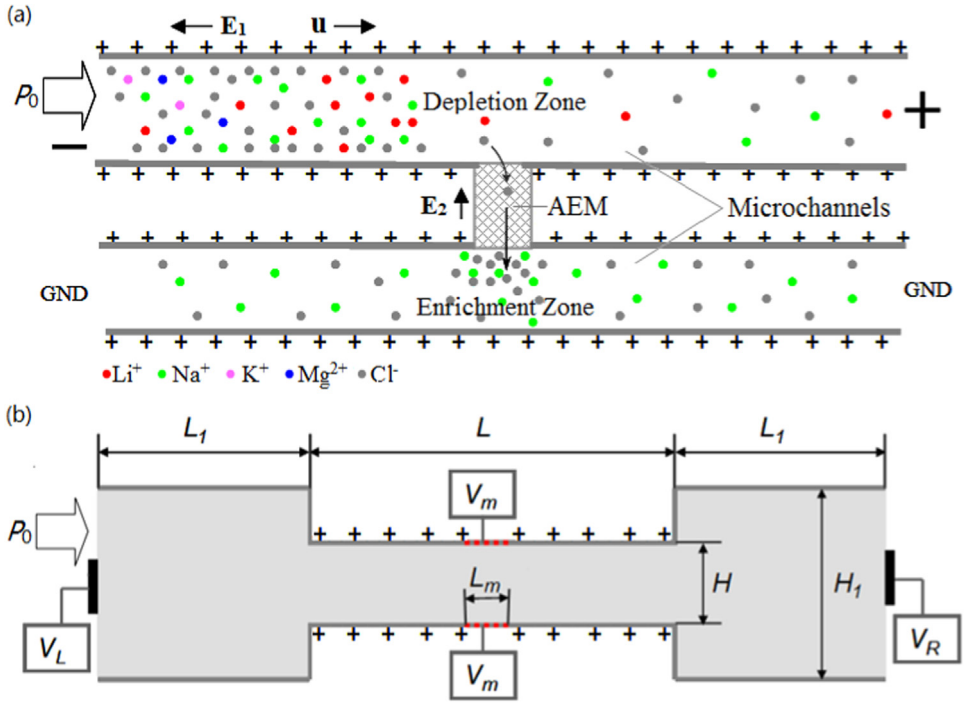

Fig. 1. (a) System setup of a dual-channel device for ICP-based Li^+ extraction. (b) The simulation model.

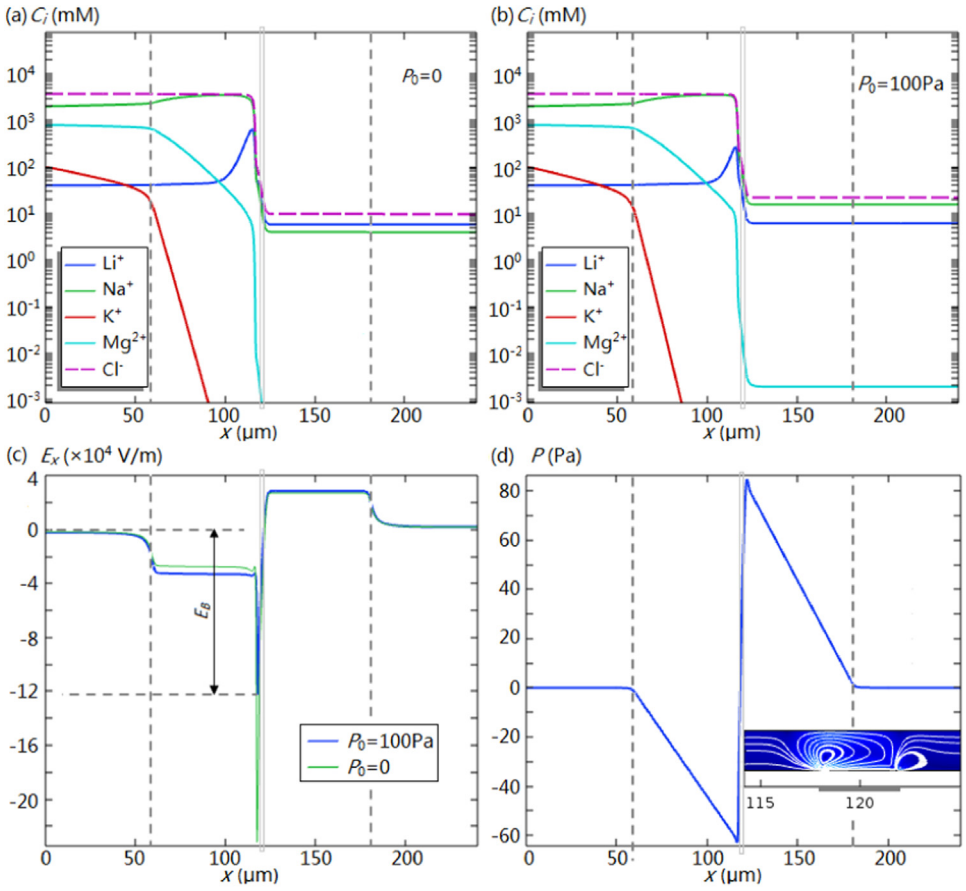

Fig. 2. (a) Steady-state concentration of ions along the centerline of the channel at $V_{cm}=100V_T$ and $P_0 = 0$. The narrow gray box at 118–122 μm depicts the location of the membrane, whereas the dashed vertical lines show the location of intersection between the microchannel and the wider compartments. (b) Concentration profiles at $V_{cm}=100V_T$ and $P_0 = 100$ Pa. (c) Distribution of tangential electric field (E_x) along the centerline of the channel. The strength of the electric field barrier is described by E_B. (d) Distribution of pressure along the centerline of the microchannel at $V_{cm}=100V_T$, $P_0 = 0$. Vortexes induced by EOF2 are shown in the inset, with the background color depicting the magnitude of the fluid flow.

$$\mathbf{J}_i = -(D_i\nabla C_i + Z_i(D_iF/RT)C_i\nabla\Phi) + \mathbf{U}C_i, \quad (4)$$

$$-\nabla\cdot(\varepsilon\nabla\Phi) = \rho_e. \quad (5)$$

Here, **U** is the velocity of the fluid, P is the pressure, and Φ is the electric potential. C_i and $\mathbf{J_i}$ are concentration and flux of species i, respectively. For convenience, we set $i = 1$ for Li^+, $i = 2$ for Na^+, $i = 3$ for K^+, $i = 4$ for Mg^{2+}, and $i = 5$ for Cl^-, respectively. Z_i represents the valance of species i ($Z_1 = Z_2 = Z_3 = 1$, $Z_4 = 2$, $Z_5 = -1$). $\rho_e = e\sum_{i=1}^{5} Z_iC_i$ is the free space charge density, where e is the elementary charge. Parameters ρ, η and ε are the mass density, dynamic viscosity and dielectric permittivity of the solution, respectively. $T = 300$ K is the temperature. Constants F and R are Faraday's constant and gas constant, respectively.

2.3. Boundary conditions

The boundary conditions of system are as follows [39,44,45].

At the membrane surfaces, it is assumed that: (i) fluxes of cations across the membrane are zero; (ii) the concentration of Cl^- at the membrane surface is C_m; (iii) the electric potential at the membrane surface is V_m; (iv) the membrane is impermeable to fluid and no-slip conditions are valid. The corresponding equations are:

$$C_5 = C_m,\ \Phi = V_m,\ \mathbf{U} = \mathbf{0},\ \mathbf{J}_i\cdot\mathbf{n} = 0,\ i = 1,\ \ldots,4. \quad (6)$$

where **n** is the normal vector perpendicular to the boundary pointing out of the fluid domain. At microchannel walls the boundary conditions are: (i) constant surface charge density σ_+; (ii) no-slip condition for fluid velocity; (iii) impermeability to all anions and cations:

$$\nabla\Phi\cdot\mathbf{n} = \sigma_+/\varepsilon,\ \mathbf{U} = \mathbf{0},\ \mathbf{J}_i\cdot\mathbf{n} = 0,\ i = 1,\ \ldots,5. \quad (7)$$

At the inlet boundary: (i) concentration of all ions are the same as those in the inlet reservoir; (ii) the electric potential is V_L; (iii) the pressure is P_0:

$$\Phi = V_L,\ \nabla\mathbf{U}\cdot\mathbf{n} = \mathbf{0},\ P = P_0,\ C_i = C_{i,0},\ i = 1,\ \ldots,5. \quad (8)$$

At outlet boundary: (i) free boundary conditions are applied for fluid flow; (ii) the electric potential is set to V_R.

$$\Phi = V_R,\ \nabla\mathbf{U}\cdot\mathbf{n} = \mathbf{0},\ P = 0,\ \nabla C_i\cdot\mathbf{n} = 0,\ i = 1,\ \ldots,5. \quad (9)$$

At reservoirs walls: (i) no-slip condition for fluid velocity; (ii) zero charge.

$$\mathbf{U} = \mathbf{0},\ \nabla\Phi\cdot\mathbf{n} = 0. \quad (10)$$

3. Results and discussions

In our simulation, the geometric parameters of the microfluidic channel are $L = 120$ μm, $H = 4$ μm, $L_1 = H_1 = 60$ μm, and $L_m = 4$ μm (see Fig. 1(b)). The charge density on the surfaces of microchannel walls is $\sigma_+ = 5$ mC/m^2. The ion concentrations at the inlet reservoir (the left boundary of the model) are set to be equal to the ion concentrations in West Taijinaier Lake in China [40], i.e. $C_{1,0} = 0.04$ M (Li^+), $C_{2,0} = 2$ M (Na^+), $C_{3,0} = 0.1$ M (K^+), $C_{4,0} = 0.8$ M (Mg^{2+}), and $C_{5,0} = 3.74$ M (Cl^-). The concentration of Cl^- on the membrane surface is set as $C_m = 10$ mM [41]. The diffusion coefficients of the ions are $D_1 = 1.03\times10^{-5}$ cm^2/s (Li^+), $D_2 = 1.333\times10^{-5}$ cm^2/s (Na^+), $D_3 = 1.957\times10^{-5}$ cm^2/s (K^+), $D_4 = 0.706\times10^{-5}$ cm^2/s (Mg^{2+}), and $D_5 = 2.032\times10^{-5}$ cm^2/s (Cl^-) [43]. Voltages of $V_L = 0$ and $V_R = 20V_T$ are applied to the left and right boundaries, respectively, with $V_T = 25.8$ mV being the thermal voltage. The external pressure at the left boundary P_0 and the voltage at the membrane surface V_m (presented in the form of V_{cm}) are varied. Because of the abundance of Na^+ in the brine, and the ease of separating Li^+ from Na^+ (by reaction with sodium carbonate and collection of the precipitated Li_2CO_3 in subsequent steps), the concentration of Na^+ is not an important metric in this

study. Instead, special attention is paid to the quantity of Li^+ extracted, indicated by the flux of Li^+ over the microchannel, and the quality indicated by Li^+/Mg^{2+} flux ratio.

The governing Eqs. (1)–(5) are solved with the specified boundary conditions (6 − 10) using COMSOL v5.2a. Detailed description of the numerical methods could be find in Ref. 31. Steady state solutions are obtained to study the behaviors of the system. Effects of cross-membrane voltage V_{cm} and the external pressure P_0 on the performance of lithium extraction in the continuous running mode are analyzed, in terms of Li^+ flux, Li^+/Mg^{2+} ratio etc.

3.1. Mechanism of ICP-based microfluidic Li^+ extraction

Firstly, we simulate the steady-state behavior of the system at $V_{cm} = 100V_T$, without applying an external pressure ($P_0 = 0$). In this case, all processes, including the fluid flow, transport of ion species, and distribution of electric potential, are driven by the electric field. Fig. 2(a) shows the steady-state ion concentrations along the centerline of the microchannel. One may find that the selective transport of Cl^- out of the microchannel at the membrane location ($118\,\mu m < x < 122\,\mu m$) decreases the concentration of Cl^-, as well as all the cation species, to very low levels. This low concentration region, or the ion depletion zone, expands to the downstream microchannel ($x > 122\,\mu m$) following the fluid flow. Inside the upstream microchannel ($60\,\mu m < x < 118\,\mu m$), significant enrichment of Li^+ takes place (see the blue curve in Fig. 2(a)). The maximum concentration of Li^+ is 0.65 M, which is 16 times of its value in the inlet reservoir (0.04 M). In contrast, the concentration of Na^+ is slightly increased by 76.6% to 3.53 M, whereas Mg^{2+} and K^+ are significantly depleted. In addition, because focused band of Li^+ occupies the majority of the near-membrane space in upstream microchannel, Li^+ has more chances to overcome the electric field barrier to flow into the downstream channel than other cations. Therefore, in the downstream channel, the concentration of Li^+ is highest (0.006 M), which is 1.5 times of that of Na^+ (0.004 M). In terms of Li^+ extraction, under conditions of $P_0 = 0$ and $V_{cm} = 100V_T$, an average fluid flow velocity of 1.44 mm/s and Li^+ flux of 1.45×10^{-2} mol/m^{2}s are achieved. Dividing this Li^+ flux by the convective flux of Li^+ in the original brine ($C_{1,0} = 0.04$ M) at the same velocity, one knows that only 25.3% of Li^+ in the original brine flows into the right reservoir.

In contrast to the mild differences in the diffusion coefficients (ranging from 0.706×10^{-5} cm^2/s to 1.957×10^{-5} cm^2/s) and the valences (either 1 or 2) of the four cation species, their concentration profiles as shown in Fig. 2(a) are surprisingly different. At $V_{cm} = 100V_T$, Li^+ ions are sharply focused with a bell-shaped peak at the front of the ion depletion zone near the membrane, while Na^+ ions are very slightly enriched with a concentration plateau occupying most of upstream microchannel. In contrast, Mg^{2+} and K^+ are depleted to different extents. Generally, these diversified distributions are determined by three tightly coupled mechanisms: (1) the diverse balance between the rightward fluid drag force F_D and the leftward electrophoretic F_E applied to different ions; (2) the charge neutrality among cations and anions in the solution; and (3) the competition between the co-charged ions inside the microchannel in the ICP environment. These mechanisms work together to determine the dynamics of each cation species and the behavior of the system. For simplicity, we present these mechanisms in one-dimensional (1D) description. Although some phenomena is intrinsically 2D (e.g. vortexes), they are not expected to affect the validities of these fundamental mechanisms.

Firstly, the balance between F_E and F_D determines whether a cation species could be focused and where its potential focusing location is. In one dimensional (1D) description, for cation species i in a fluid flowing at a velocity $\bar{u}$ and under electric field E_x, the electrophoretic force and the fluid drag force are $F_{E,i} = Z_i F|E_x|$ and $F_{D,i} = \bar{u}\, RT/D_i$, respectively. The ratio $\alpha_i = F_{E,i}/F_{D,i}$ determines the direction of moving for the ion at a specific location. It will move leftward if $\alpha_i > 1$, but rightward if $\alpha_i < 1$, targeting at a quasi-equilibrium location (where $\alpha_i = 1$ is satisfied) if such a location exists [42]. Noticing that the electrophoretic mobility of cation species i is $\mu_{e,i} = Z_i F D_i/RT$, the ratio α_i could be expressed as $\alpha_i = \mu_{e,i}|E_x|/\bar{u}$. Thinking of the dynamics of different ions at a specific location with specified E_x and $\bar{u}$, one may find that each ion species moves according to its own force balance (α value). Because α for an ion species is proportional to its electrophoretic mobility μ_e, cation species with higher mobilities have higher α values, and thus have a stronger tendency to move leftward, while those with lower mobilities have lower α values and have a stronger tendency to move rightward. If we follow a specific ion with a given μ_e, its α value is determined by $|E_x|$, because the fluid velocity $\bar{u}$ is constant in a 1D microchannel in steady state. The ion has a tendency to migrate to the quasi-equilibrium location with $\alpha = 1$, where the electric field strength is $|E_x| = \bar{u}/\mu_e$. For different cation species migrating in a solution with the same fluid flow velocity $\bar{u}$ value and under the same electric field E_x, the species with lower electrophoretic mobilities tend to be focused at locations with higher electric field strengths. From mobilities of Li^+, Na^+, Mg^{2+} and K^+, which are 4.007×10^{-8} m^2/Vs, 5.190×10^{-8} m^2/Vs, 5.493×10^{-8} m^2/Vs and 7.616×10^{-8} m^2/s respectively [43], we know that Li^+ ions tend to focus at a location with highest $|E_x|$, whereas K^+ ions tend to focus at a location with lowest $|E_x|$. In our system, $|E_x|$ increases monotonically in the upstream microchannel to a maximum value, with a significant increase at the entrance, a flat region in the middle and a sharp increase at the front of ion depletion zone (see Fig. 2(c). Therefore, Li^+ ions are focused at a location closest to the membrane, where the electric field is stronger, whereas Na^+ ions are focused at a location with weaker electric field, which lies further in the upstream microchannel. As for Mg^{2+} and K^+, $|E_x|$ is so high that their values of α are greater than 1.0 in the whole upstream microchannel, thus they are not focused. Because K^+ ions have the largest electrophoretic mobility, their tendency to move leftward is the strongest, thus they are most depleted. It is noteworthy as well that while the ratio of F_E to F_D determines whether an ion species could be focused and where its potential focusing location is, the magnitudes of these forces determine compactness of the focused peak. Higher F_E and F_D values produce narrower peaks because forces that push the ion back to its quasi-equilibrium location are stronger if the ion moves away. That is the reason why the concentration profile of Li^+ has a sharp peak.

Secondly, the maximum concentrations of the focused ions are affected by the maximum electric field strength in front of the depletion zone, and is limited by the neutrality condition [46]. The maximum electric field strength, $E_B = \max(-E_x)$ as depicted in Fig. 2(c), determines the maximum electric force that hinders the convective transport of cations through the ion depletion zone. It is a direct measure of the energy barriers, which determines the maximum concentration of the ions in the upstream channel and their chances to pass through depletion zone and flow into the downstream. In this sense, E_B is referred to as the electric field barrier. Higher E_B will produce higher peak concentration for specific cations. Meanwhile, the maximum concentrations of focused ions are limited by the neutrality condition, i.e. the total charge densities of the cations must be equal to that of the anions in the microchannel. In Fig. 2(a), total concentration of the focused Li^+ and Na^+ (and the depleted Mg^{2+} and K^+) is limited by that of Cl^-, which is actually slightly lower than that in the inlet reservoir (see Ref. 31). When more ions are carried into the microchannel after their peak concentrations reach the limits determined by neutrality condition, their peaks will expand to the upstream instead of growing in height. This is the reason why a plateau is formed in concentration profile of Na^+.

Lastly, the neutrality condition gives rise to the third mechanism in this system, i.e. competition between the co-charged cations. At any location, focusing of one species of lower mobility must reduce concentrations of other co-charged species of higher mobilities, simply because their total charge densities is limited. As a result, ions with higher mobilities are partially replaced by those with lower mobilities

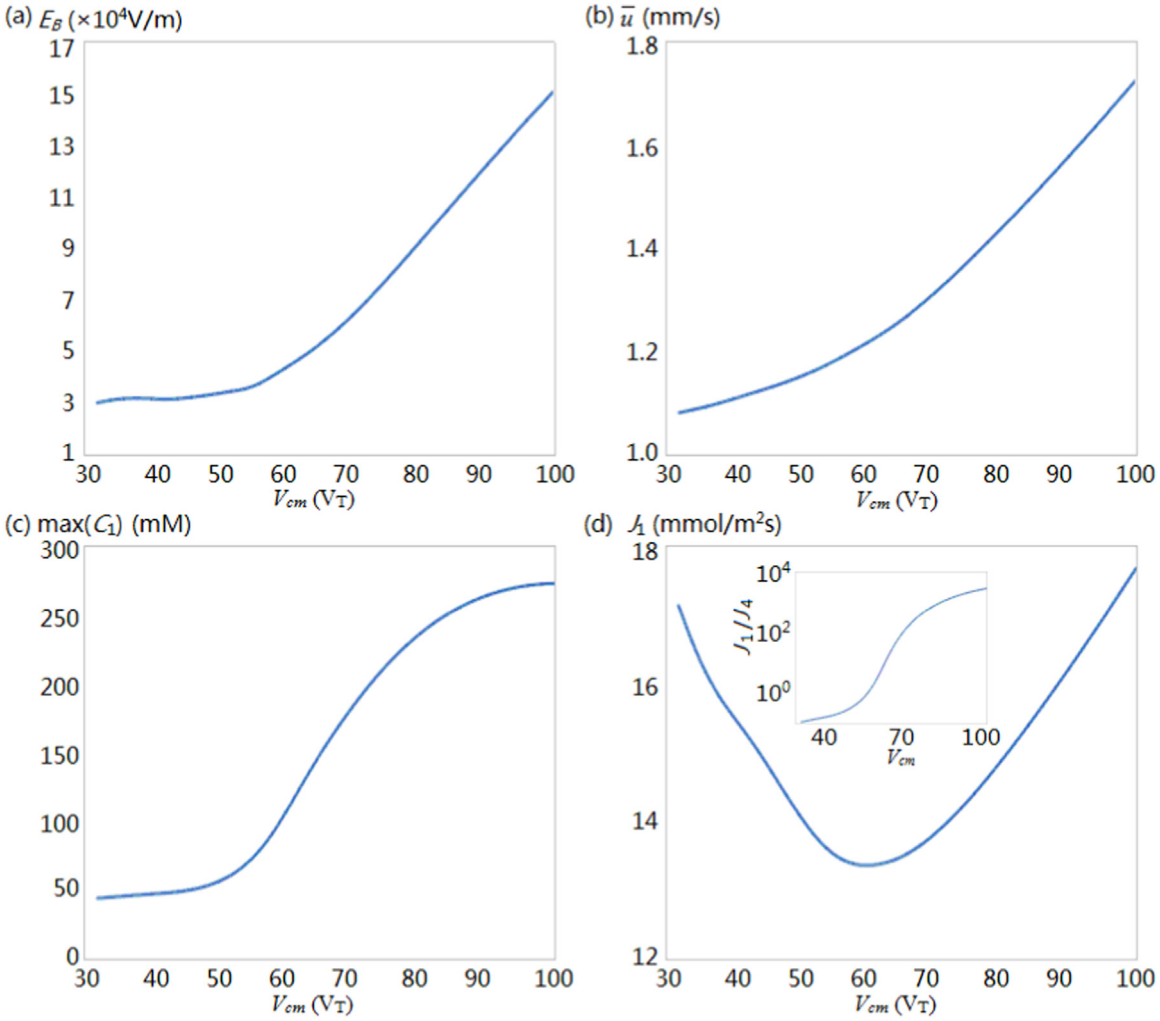

Fig. 3. Dependences of (a) electric field barrier, (b) average fluid flow velocity, (c) the maximum Li^+ concentration in the upstream channel, and (d) the flux of Li^+ on the cross-membrane voltage at P_0 = 100 Pa.

[31], the extent of which is determined by the local electric field, mobility differences between competing ions etc. Among all the cation species, mobility of K^+ is the highest, thus K^+ ions have to give way to all other ions inside the microchannel in an ICP environment, including Mg^{2+}. The concentration and the flux of K^+ ions are therefore reduced to extremely low values.

In addition to the ion depletion and the strong electric field, selective transport of Cl^- also induces the electroosmotic flow of the second kind (EOF2) near the upstream side of the membrane [45]. This EOF2 increases the pressure in the downstream channel, decreases the pressure in the upstream, and generates a pair of vortices near the membrane location (see Fig. 2(d), where only part of the lower half channel is shown) [44]. In this system, EOF2 flows act as additional pumps that drive fluid flow in this system [31,45].

Generally, when such a system is driven merely by the electric field (P_0 = 0), ion depletion effect reduces the concentrations and fluxes of all ions to very low levels in the downstream microchannel. In order to increase the throughput, an external pressure P_0 = 100 Pa is applied to the inlet. The increased fluid flow carries more cations to enter the microchannel and pass the lowered electric field barrier (c.f. Section 3.3). Consequently, concentrations of all ion species in the downstream microchannel are increased significantly (see Fig. 2(b)). For example, the concentration of Li^+ in the downstream microchannel at P_0 = 100 Pa is 6.17 mM, about 1.06 times higher than that at P_0 = 0 (5.78 mM). Meanwhile, the concentration of Na^+ in the downstream channel is 15.7 mM at P_0 = 100 Pa, which is about 3.9 times of that at P_0 = 0 (4 mM). Concentrations of Mg^{2+} (0.0019 mM) and K^+ (10^{-11} mM) are also significantly increased, but their values are still far below those of Na^+ and Li^+. The average fluid flow velocity is 1.72 mm/s, which is about 1.2 times of that at P_0 = 0 (1.44 mm/s). The fluxes of Li^+ and Mg^{2+} at P_0 = 100 Pa are 1.77×10^{-2} mol/m²s and 6.28×10^{-6} mol/m²s, which are 1.22 and 18.5 times of their corresponding values at P_0 = 0, respectively. In terms of Li^+ extraction, the application of P_0 = 100 Pa increases the fluid flow velocity to 1.2 times and the Li^+ flux to 1.22 times of their values at P_0 = 0. However, the Li^+/Mg^{2+} flux ratio is reduced to 2.81×10^3, which is 6.59×10^{-2} times of its value at P_0 = 0 (4.27×10^4). In this scenario, about 25.6% of Li^+ in the brine flow into the right reservoir, with a Li^+/Mg^{2+} flux ratio of 2.81×10^3.

3.2. Effects of cross-membrane voltage

As the driving factor that induces ICP, the cross-membrane voltage V_{cm} plays a crucial role in this system. Increasing V_{cm} drives more Cl^- ions out of the channel through AEMs, thus resulting in lower concentrations in the ion depletion zone and a higher E_B. This trend is clearly demonstrated in Fig. 3(a), where the relationship between E_B and V_{cm} is depicted at P_0 = 100 Pa. Under low V_{cm} (< 60V_T), ion depletion effect is insignificant. The conductivity of the solution does not change much and the electric field barrier grows very slowly. However,

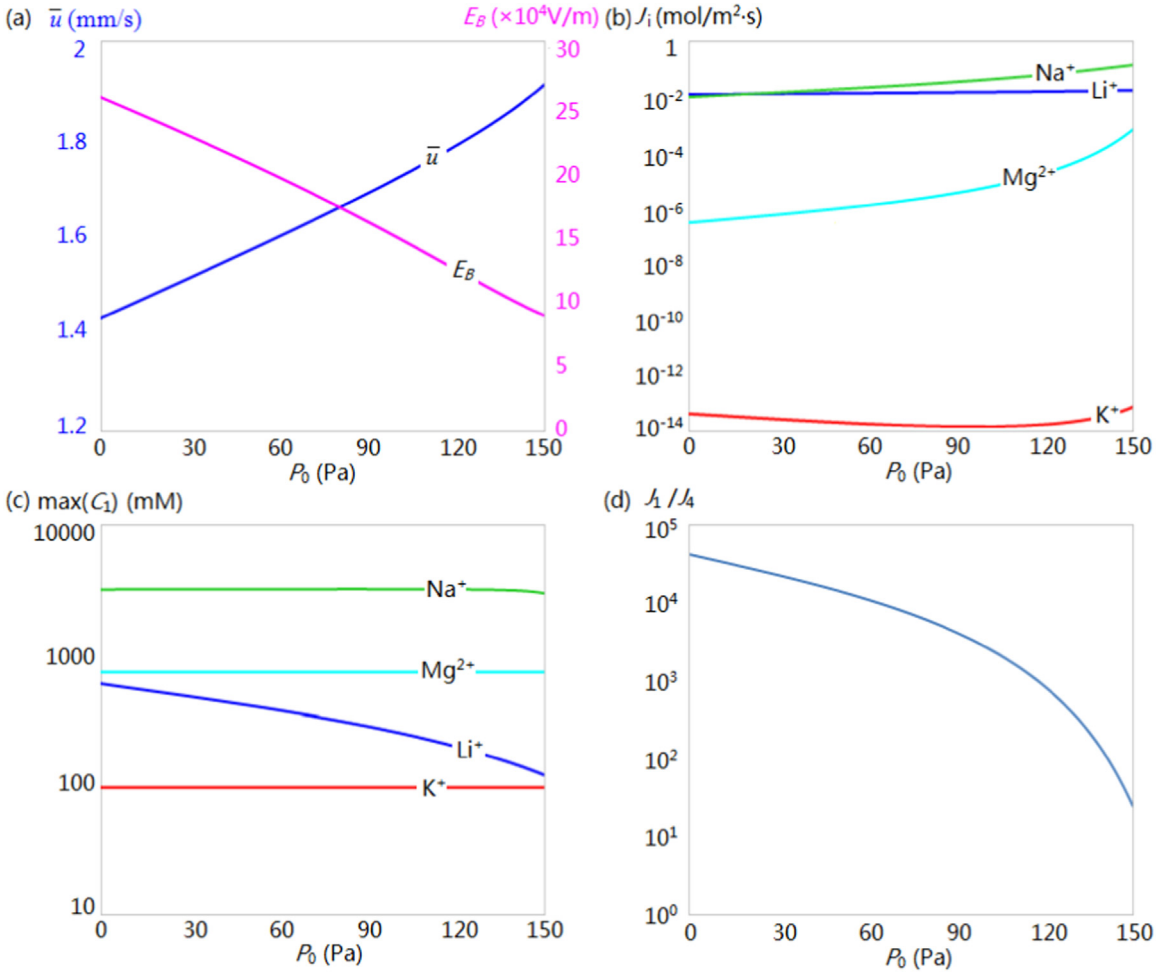

Fig. 4. Dependences of (a) electric field barrier E_B and average fluid flow velocity $\bar{u}$, (b) fluxes of cation species, (c) maximum concentrations of cation species in the upstream channel, and (d) the Li^+/Mg^{2+} flux ratio on the external pressure P_0 at $V_{cm}=100V_T$.

under high V_{cm} ($\geq 60V_T$), ion depletion is fully developed and E_B increases with V_{cm}, almost linearly. It is noteworthy that when V_{cm} increases by 3.12 times from $32V_T$ to $100V_T$, E_B increases by 5.01 times from 3.01×10^4 V/cm to 1.51×10^5 V/cm.

Fig. 3(b) shows the relationship between the average fluid flow velocity $\bar{u}$ and cross-membrane voltage V_{cm} at $P_0 = 100$ Pa. It is clear that $\bar{u}$ increases with V_{cm} moronically. This is because a higher V_{cm} induces a stronger tangential electric field $\mathbf{E_1}$ in the upstream channel, therefore produces faster EOF1. Meanwhile, a higher V_{cm} induces higher extended space charges near the membrane surface, which generates stronger EOF2 and pumping more fluids downstream. Again, under high V_{cm}, $\bar{u}$ increases linearly with V_{cm}. While under low V_{cm}, $\bar{u}$ increases at a slower rate. When V_{cm} increases from $32V_T$ to $100V_T$, $\bar{u}$ increases by 1.59 times from 1.08 mm/s to 1.72 mm/s.

When V_{cm} is increased, higher E_B imposes stronger electrophoretic force on cations at the front of depletion zone in the upstream channel, which promotes the trapping of the cations. In addition, the increased $\bar{u}$ imposes stronger drag forces that drive cations to overcome the electric field barrier and leak into the downstream channel. Generally, the effect of electric field outweighs that of the fluid drag, which produces an increasing concentration of Li^+ in the enrichment zone at a constant pressure. As shown in Fig. 3(c), at $P_0 = 100$ Pa, when V_{cm} increases from $32V_T$ to $100V_T$, the maximum Li^+ concentration rises from 43.9 mM to 270.9 mM. Differences in the dependencies of E_B and $\bar{u}$ on V_{cm} result in a complicated trend for Li^+ flux (See Fig. 3(d)). At $P_0 = 100$ Pa, Li^+ flux firstly decreases from 1.71×10^{-2} mol/m²s at $V_{cm}=32V_T$ to 1.34 mol/m²s at $V_{cm}=65V_T$, and then increases, still almost linearly at $V_{cm} > 65V_T$. As for Li^+/Mg^{2+} flux ratio, it increases with V_{cm} drastically. In contrast to the narrow range of the Li^+ flux, from 1.34×10^{-2} mol/m²s to 1.72×10^{-2} mol/m²s when V_{cm} changes from $32V_T$ to $100V_T$, the Li^+/Mg^{2+} flux ratio increases considerably from 0.12 to 2815, by 2.44×10^4 times.

It is noteworthy that the 4th-order increase in Li^+/Mg^{2+} flux ratio is largely caused by the decrease of Mg^{2+} flux, because Li^+ flux is varied in a very narrow range (see Fig. 3(d)). As shown in Fig. 3(a) and Fig. 3(b), when V_{cm} increases from $32V_T$ to $100V_T$, $|E_x|$ increases by 5.01 times, while $\bar{u}$ increases by 1.59 times merely. This yields an increase of α by 3.15 times. Because α value of Mg^{2+} is greater than 1 even at $V_{cm}=32V_T$, increasing α by 3.15 times generates a much stronger tendency for Mg^{2+} to move leftward. This effect, along with the repelling forces from the more focused Na^+ and Li^+ ions, leaves an extremely low concentration of Mg^{2+} inside the microchannel under high V_{cm}. Compared with Mg^{2+}, these effects are more significant for K^+ (because μ_e of K^+ is higher than that of Mg^{2+}), so the concentration of K^+ is even lower.

3.3. Effect of external pressure

The application of the external pressure P_0 promotes the fluid flow. As shown by the blue curve in Fig. 4(a), when P_0 increases from 0 to 150 Pa at $V_{cm}=100V_T$, the average flow velocity increases from 1.4 mm/s to 1.9 mm/s. A faster fluid flow carries more ions to the membrane region, increases the ion concentrations there, and thus weakens the electric field barrier at the front of the depletion zone (see

the magenta curve in Fig. 4(a)). These changes both contribute to the higher fluxes of all cation species, although the magnitudes of the changes differ significantly (see Fig. 4(b)). More specifically, the fluxes of Li^+, Na^+, K^+, and Mg^{2+} at $P_0 = 150$ Pa are 1.4, 15.7, 1.8, and 2386.8 times of their corresponding values at $P_0 = 0$, respectively. Surprisingly, the flux of Li^+, which has the highest ratio of fluid drag force to electrophoretic force, experiences the smallest magnitude of increasing. This is because as P_0 increases, E_B is decreased, causing the maximum concentration of Li^+ in the upstream channel to decrease significantly (see Fig. 4(c)). Multiplication of the increased fluid velocity and the decreased Li^+ concentration produces a very slowly increased convective flux of Li^+. In contrast, changes in the maximum concentrations of Na^+, K^+ and Mg^{2+} in the upstream microchannel are less significant (see Fig. 4(c)). Their fluxes increase with the faster fluid flow velocity and the lower E_B significantly. A mildly increasing Li^+ flux and sharply increasing Mg^{2+} flux, produces an exponential decreasing of Li^+/Mg^{2+} ratio (see Fig. 4(d)). In fact, increasing P_0 from 0 to 150 Pa will decrease the Li^+/Mg^{2+} flux ratio by 1.7×10^4 times. In an optimal design, it is desirable to maximize the Li^+ flux while keeping Li^+/Mg^{2+} flux ratio above a value specified by the requirements of the product.

One may notice that the flux of K^+ as shown in Fig. 4(b) is at least $\sim 10^7$ times lower than that of Mg^{2+}. This difference is huge in the sense that the concentration of K^+ in the brine is 100 mM, only 8 times lower than that of Mg^{2+} (800 mM), and the mobility of K^+ is only 1.39 times higher than that of Mg^{2+}. This huge flux difference is caused by the extremely low concentration of K^+ inside the microchannel, as well as the highest tendency to move leftward (c.f. Section 3.1).

4. Conclusions

In this paper, we propose a novel device for the extraction of Li^+ from high Mg^{2+}/Li^+ ratio brines. In the proposed system, we tune the electric field barrier by ICP and an external pressure to allow for the passage of Li^+ and Na^+ while retaining most of Mg^{2+} and K^+, thereby realizing the continuous extraction of Li^+ from brines. The mechanism of this device is demonstrated through 2D numerical simulations. The flux of Li^+ and the Li^+/Mg^{2+} flux ratio are analyzed with varied cross-membrane voltages and external pressures. It is found that the application of an external pressure 100 Pa under $V_{cm} = 100 V_T$ induces slow increasing of the fluid flow velocity (~1.2 times) and faster increasing of Li^+ flux (one order higher), but at the cost of the exponential decreasing of the Li^+/Mg^{2+} flux ratio. Under an given external pressure, increase of V_{cm} in the low V_{cm} regime may induce lower fluid flow velocities and lower Li^+ fluxes, due to the relatively smaller increase in EOF1 in the upstream microchannel and larger decrease in EOF1 in the downstream. In the high V_{cm} regime, Li^+ flux increase with V_{cm} exponentially. The Li^+/Mg^{2+} ratio under an external pressure generally increases exponentially with V_{cm}, but the increase rate is very slow in low V_{cm} regime.

This method does not involve chemical reactions of ions in the brine, and it blocks the passage of Mg^{2+} through localized strong electrophoretic forces. The typical channel size is in the order of tens of micrometers, therefore it does not suffer from the problem of clogging. Although our results are obtained using a simple 2D simulation model and a high concentration brine, the fundamental mechanism is clearly demonstrated. These results and knowledge provide important guidance to the design and implementation of actual systems, not only for Li^+ extraction, but also for other ionic or molecular separation tasks, especially when both the ICP phenomena and the external pressures are involved.

Although dilute solutions of electrolytes were used in most studies for the ICP phenomena, ion depletion in a microchannel filled with highly concentrated solutions had been readily implemented in 2010, when Kim et al. used dual-channel devices to desalinate seawater brines [24]. We believe ICP could also be realized in the actual lithium extraction system, and the fundamental mechanisms presented here are valid, despite the fact that the results in this paper are obtained totally from numerical simulations.

Acknowledgments

This work is supported by the National Natural Science Foundation of China [Grant Nos. 11372229, 21576130, 21490584]; the National Institutes of Health of the United States[Grant No. U19AI109755].

References

[1] B. Scrosati, J. Hassoun, Y.K. Sun, Lithium-ion batteries. A look into the future, Energ. Environ. Sci. 4 (2011) (32 87-32 95).
[2] S.E. Kesler, P.W. Gruber, P.A. Medina, G.A. Keoleian, M.P. Everson, T.J. Wallington, Global lithium resources: relative importance of pegmatite, brine and other deposits, Ore. Geol. Rev. 48 (2012) 55–69.
[3] P.W. Harben, G.H. Edwards, The global lithium industry: a portrait of rapid flux, Jom 49 (1997) 21–22.
[4] Z.Y. Ji, Q.B. Chen, J.S. Yuan, J. Liu, Y.Y. Zhao, W.X. Feng, Preliminary study on recovering lithium from high Mg2+ /Li+, ratio brines by electrodialysis, Sep. Purif. Technol. 172 (2017) 168–177.
[5] P.K. Choubey, K.S. Chung, M.S. Kim, J.C. Lee, R.R. Srivastava, Advance review on the exploitation of the prominent energy-storage element Lithium. Part II: from sea water and spent lithium ion batteries (LIBs), Miner. Eng. 110 (2017) 104–121.
[6] C.W. Hwang, M.H. Jeong, Y.J. Kim, W.K. Son, K.S. Kang, C.S. Lee, T.S. Hwang, Process design for lithium recovery using bipolar membrane electrodialysis system, Sep. Purif. Technol. 166 (2016) 34–40.
[7] J. Nan, D. Han, X. Zuo, Recovery of metal values from spent lithium-ion batteries with chemical deposition and solvent extraction, J. Power Sources 152 (2005) 278–284.
[8] S.E. Kesler, P.W. Gruber, P.A. Medina, G.A. Keoleian, M.P. Everson, T.J. Wallington, Global lithium resources: relative importance of pegmatite,brine and other deposits, Ore. Geol. Rev. 48 (2012) 55–69.
[9] Z. Zhou, Q. Wei, W. Fei, Extraction equilibria of lithium with tributyl phosphate in three diluents, J. Chem. Eng. Data 56 (2011) 3518–3522.
[10] L.X. Yang, S.X. Wu, X.L. Liu, J. He, W.G. Chen, Lithium and magnesium separation from salt lake brine by tributyl phosphate under action of co-extraction reagent ClO4−, Chem. J. Chin. Univ. 34 (2013) 55–60.
[11] T. Wajima, K. Munakata, T. Uda, Adsorption behavior of lithium from seawater using manganese oxide adsorbent, Plasma Fusion Res. 7 (2012) (2405021-2405021).
[12] H.J. Hong, I.S. Park, J. Ryu, T. Ryu, B.G. Kim, K.S. Chung, Immobilization of hydrogen manganese oxide (HMO) on alpha-alumina bead (AAB) to effective recovery of Li+ from seawater, J. Chem. Eng. 271 (2015) 71–78.
[13] C. Özgür, Preparation and characterization of LiMn2O4, ion-sieve with high Li+, adsorption rate by ultrasonic spray pyrolysis, Solid State Ion. 181 (2010) 1425–1428.
[14] Z. Zhao, X. Si, X. Liu, L. He, X. Li, Li extraction from high Mg/Li ratio brine with LiFePO4 /FePO4, as electrode materials, Hydrometallurgy 133 (2013) 75–83.
[15] Y. Li, Z. Zhao, X. Liu, X. Chen, Extraction of lithium from salt lake brine by aluminum-based alloys, Chin. J. Inorg. Chem. 25 (2011) 3484–3489.
[16] C. Shi, Y. Jia, C. Zhang, H. Liu, Y. Jing, Extraction of lithium from salt lake brine using room temperature ionic liquid in tributyl phosphate, Fusion Eng. Des. 90 (2015) 1–6.
[17] P. Chen, S. Tang, H. Yue, C. Liu, C. Li, B. Liang, Lithium enrichment of high Mg/Li ratio brine by precipitation of magnesium via combined CO_2 mineralization and solvent extraction, Ind. Eng. Chem. Res. 56 (2017).
[18] T. Hoshino, Development of technology for recovering lithium from seawater by electrodialysis using ionic liquid membrane, Fusion Eng. Des. 88 (2013) 2956–2959.
[19] T. Hoshino, Innovative lithium recovery technique from seawater by using world-first dialysis with a lithium ionic superconductor, Desalination 359 (2015) 59–63.
[20] X. Nie, S. Sun, Z. Sun, X. Song, J. Yu, Ion-fractionation of lithium ions from magnesium ions by electrodialysis using monovalent selective ion-exchange membranes, Desalination 403 (2016) 128–135.
[21] P.K. Choubey, M.S. Kim, R.R. Srivastava, J.C. Lee, J.Y. Lee, Advance review on the exploitation of the prominent energy-storage element: lithium. Part I: from mineral and brine resources, Miner. Eng. 89 (2016) 119–137.
[22] Q. Pu, J. Yun, H. Temkin, S. Liu, Ion-enrichment and ion-depletion effect of nanochannel structures, Nano Lett. 4 (2004) 1099–1103.
[23] A.V. Virkar, J. Chen, C.W. Tanner, J.W. Kim, The role of electrode microstructure on activation and concentration polarizations in solid oxide fuel cells, Solid State Ion. 131 (2000) 189–198.
[24] S.J. Kim, S.H. Ko, K.H. Kang, J. Han, Direct seawater desalination by ion concentration polarization, Nat. Nanotech. 5 (2010) 297.
[25] V. Nikonenko, A.V. Kovalenko, M.K. Urtenov, N.D. Pismenskaya, J. Han, P. Sistat, G. Pourcelly, Desalination at overlimiting currents: state-of-the-art and perspectives, Desalination 342 (2014) 85–106.
[26] D. Deng, W. Aouad, W.A. Braff, S. Schlumpberger, M.E. Suss, M.Z. Bazant, Water purification by shock electrodialysis: deionization, filtration, separation, and disinfection, Desalination 357 (2015) 77–83.

[27] P.H. Chiu, C.C. Chang, R.J. Yang, Electrokinetic micromixing of charged and non-charged samples near nano–microchannel junction, Microfluid Nanofluid 14 (2013) 839–844.
[28] S.J. Lee, D. Kim, Millisecond-order rapid micromixing with non-equilibrium electrokinetic phenomena, Microfluid Nanofluid 12 (2012) 897–906.
[29] Y. Wang, A.L.S. And, J. Han, Million-fold preconcentration of proteins and peptides by nanofluidic filter, Anal. Chem. 77 (2005) 4293–4299.
[30] C.C. Lin, J.L. Hsu, G.B. Lee, Sample preconcentration in microfluidic devices, Microfluid Nanofluid 10 (2011) 481–511.
[31] Z. Li, W. Liu, L. Gong, Y. Zhu, X. Lu, Y. Gu, J. Han, Accurate multi-physics numerical analysis of particle preconcentration based on ion concentration polarization, Int, J. Appl. Mech. 9 (2017) 1750107.
[32] W. Ouyang, J. Han, W. Wang, Enabling electrical biomolecular detection in high ionic concentrations and enhancement of detection limit thereof by coupling nanofluidic crystal with reconfigurable ion concentration polarization, Lab Chip 17 (2017) 3772–3784.
[33] S.Y. Son, S. Lee, H. Lee, S.J. Kim, Engineered nanofluidic preconcentration devices by ion concentration polarization, Biochip J. (2016) 1–11.
[34] W. Kim, S. Park, K. Kim, S.J. Kim, Experimental verification of simultaneous desalting and molecular preconcentration by ion concentration polarization, Lab Chip (2017).
[35] L.F. Cheow, J. Han, Continuous signal enhancement for sensitive aptamer affinity probe electrophoresis assay using electrokinetic concentration, Anal. Chem. 83 (2011) 7086.
[36] K. Rhokyun, S.J. Kim, J. Han, Continuous-flow biomolecule and cell concentrator by ion concentration polarization, Anal. Chem. 83 (2011) 7348–7355.
[37] I.I. Rubinstein, B. Zaltzman, Electro-osmotically induced convection at a permselective membrane, Phys. Rev. E Stat. Phys. Plasmas Fluids Relat. Interdiscip. Top. 62 (2000) 2238.
[38] V.S. Pham, Z. Li, K.M. Lim, J.K. White, J. Han, Direct numerical simulation of electroconvective instability and hysteretic current-voltage response of a permselective membrane, Phys. Rev. E Stat. Nonlin. Soft Matter Phys. 86 (2012) 046310.
[39] B. Zaltzman, I. Rubinstein, Electro-osmotic slip and electroconvective instability, J. Fluid Mech. 579 (2007) 173–226.
[40] C. Ji, The investigation of Mg2+/Li+ separation process by nanofiltration (in Chinese), East China University of Science and Technology, 2014.
[41] N.A. Mishchuk, P.V. Takhistov, Electroosmosis of the second kind, Colloid Surf. A. 95 (1995) 119–131.
[42] L. Gong, W. Ouyang, Z. Li, J. Han, Force fields of charged particles in micro-nanofluidic preconcentration systems, AIP Adv. 7 (2017) 125020.
[43] P. Vanýsek, Ionic conductivity and diffusion at infinite dilution (1992/93 edition), Handbook of Chemistry and Physics, CRC Press, Boca Raton, 1992.
[44] S.J. Kim, L.D. Li, J. Han, Amplified electrokinetic response by concentration polarization near nanofluidic channel, Langmuir 25 (2009) 7759–7765.
[45] W. Liu, L. Gong, Y. Zhu, Z. Li, Augmented electroosmotic flow in microchannels embedded with permselective membranes, Sci. Sin. Technol. 48 (2018) 17–24.
[46] W. Ouyang, Z. Li, X. Ye, J. Han, Theoretical limits and scaling laws for electrokinetic molecular concentration via ion concentration polarization, arXiv:1801.01462[physics.flu-dyn], 2018.